Pflugers Arch - Eur J Physiol (2009) 458:1023–1038
DOI 10.1007/s00424-009-0684-9

TMEM16B induces chloride currents activated by calcium in mammalian cells

Simone Pifferi · Michele Dibattista · Anna Menini

Received: 4 April 2009 / Accepted: 13 May 2009 / Published online: 28 May 2009

Abstract Ca^{2+}-activated Cl^- channels play important physiological roles in various cell types, but their molecular identity is still unclear. Recently, members of the protein family named transmembrane 16 (TMEM16) have been suggested to function as Ca^{2+}-activated Cl^- channels. Here, we report the functional properties of mouse TMEM16B (mTMEM16B) expressed in human embryonic kidney (HEK) 293T cells, measured both in the whole-cell configuration and in inside-out excised patches. In whole cell, a current induced by mTMEM16B was activated by intracellular Ca^{2+} diffusing from the patch pipette, released from intracellular stores through activation of a G-protein-coupled receptor, or photoreleased from caged Ca^{2+} inside the cell. In inside-out membrane patches, a current was rapidly activated by bath application of controlled Ca^{2+} concentrations, indicating that mTMEM16B is directly gated by Ca^{2+}. Both in the whole-cell and in the inside-out configurations, the Ca^{2+}-induced current was anion selective, blocked by the Cl^- channel blocker niflumic acid, and displayed a Ca^{2+}-dependent rectification. In inside-out patches, Ca^{2+} concentration for half-maximal current activation decreased from 4.9 μM at −50 mV to 3.3 μM at +50 mV, while the Hill coefficient was >2. In inside-out patches, currents showed a reversible current decrease at −50 mV in the presence of a constant high Ca^{2+} concentration and, moreover, an irreversible rundown, not observed in whole-cell recordings, indicating that some unknown modulator was lost upon patch excision. Our results demonstrate that mTMEM16B functions as a Ca^{2+}-activated Cl^- channel when expressed in HEK 293T cells.

Keywords Calcium signaling · Calcium sensitivity · Calcium-activated chloride current · Anion channel · Caged calcium · Chloride current

S. Pifferi · M. Dibattista · A. Menini (✉)
International School for Advanced Studies,
Scuola Internazionale Superiore di Studi Avanzati (SISSA),
Via Beirut 2,
34014 Trieste, Italy
e-mail: menini@sissa.it

S. Pifferi · M. Dibattista · A. Menini
Italian Institute of Technology, SISSA Unit,
Trieste, Italy

Present Address:
S. Pifferi
Max Delbrück Center for Molecular Medicine (MDC),
Berlin, Germany

Introduction

Ca^{2+}-activated Cl^- channels play several important physiological roles in many cells types, but their molecular identity has been elusive. Cl^- currents activated by intracellular Ca^{2+} were first identified in *Xenopus* oocytes [4, 37], in photoreceptor inner segments [3], in lacrimal acinar cells [34], and afterwards, many other cell types were shown to have similar types of currents. Ca^{2+}-activated Cl^- channels are involved in several physiological processes including generation of the fertilization potential in *Xenopus* oocytes; fluid secretion by exocrine glands, by airway and intestinal epithelia; regulation of cardiac excitability in cardiac myocytes; smooth muscle contraction in smooth muscle cells; and olfactory transduction in olfactory sensory neurons (for reviews see: [5, 10, 13, 25, 32, 36, 42, 43, 53]).

As for other types of ion channels, also for Ca^{2+}-activated Cl^- channels, various electrophysiological characteristics have been described and the differences could be

very important for the specific physiological roles that these proteins play in different cell types. For example, some of these channels are directly activated by Ca^{2+}, while others require also calmodulin-dependent protein kinase II for activation [2]. Moreover, the range of Ca^{2+} producing the half-maximal current varies from tens of nanomolar to micromolar concentrations (reviewed in [13]). The molecular identity of Ca^{2+}-activated Cl^- channels has been controversial, and several candidates have been proposed, including the families of bestrophins, tweety, and "Ca^{2+}-activated Cl^- channels" (CLCA; reviewed in [13, 14]). Very recently, the group of proteins named transmembrane 16 (TMEM16; also known as anoctamin) has been added to the list of molecular candidates for Ca^{2+}-activated Cl^- channels [8, 51, 54].

The recently discovered TMEM16 family is present in all eukaryotes (reviewed in [11]), and the first member was identified in 2004 by Tsutsumi and colleagues [52], while searching for candidate genes for a human hereditary disease called gnathodiaphyseal dysplasia (GDD), a rare skeletal syndrome characterized by bone fragility, sclerosis of tubular bones, and cemento-osseous lesions of the jawbone. The gene was first named GDD1 and later TMEM16E (see Table 1 of [11] for nomenclature of the human family). Additional members of the family were subsequently found by using bioinformatic tools [18–22] and, at present, ten members have been identified in mice and humans [11, 23, 49]. Furthermore, it has been shown that several human TMEM16 genes are upregulated in various types of cancer and could be valuable tumor markers [11].

Topology models indicate that TMEM16 proteins have eight putative transmembrane domains with both N- and C-terminal domains located at the intracellular side of the membrane. Although the physiological functions of these proteins are still largely unknown, it has been recently proposed that they may function as Ca^{2+}-activated Cl^- channels [8, 51, 54]. Indeed, heterologous expression of TMEM16A (also named anoctamin-1 or ANO1) in Axolotl oocytes, human embryonic kidney (HEK) 293T cells, or other cell lines, induced currents stimulated by intracellular Ca^{2+}, with anion selectivity and inhibition by several Cl^- channel blockers typical of Ca^{2+}-activated Cl^- currents. It is therefore of great interest to examine if other members of the TMEM16 family have similar functional properties. Interestingly, in a study focused on the expression cloning of the Ca^{2+}-activated Cl^- currents of *Xenopus laevis*, Schroeder et al. [51] also reported that the mouse homolog TMEM16B (mTMEM16B), generated Ca^{2+}-activated Cl^- currents in Axolotl oocytes, although the electrophysiological properties of this channel were not further investigated. At present, no other functional data have been published for other members of the TMEM16 family. Among the members of the mouse family, mTMEM16B is the most similar to mTMEM16A, with 62% amino acid identity [54]. The gene for mTMEM16B (also known as BC033409; MGC38715; Ano2) is expressed in several tissues and organs, including the retina, olfactory epithelium, pancreas, and salivary glands (see also http://symatlas.gnf.org/SymAtlas/ for a more complete list of expression). In the developing mouse nervous system, *Tmem16b* has been detected in the neural tube and in dorsal root ganglia [49]. At present, no knockout mice for this gene have yet been reported.

In humans, TMEM16B (also known as C12orf3; DKFZp434P102; anoctamin-2 or ANO2) has been shown to be involved in two types of diseases. Large deletions of TMEM16B together with von Willebrand factor genes are involved in some cases of the severe von Willebrand disease type 3, a heritable bleeding disorder that slows the blood-clotting process [50]. A recent genome-wide association study in a Japanese population indicated that single nucleotide polymorphisms located in or adjacent to gene TMEM16B were significantly associated with panic disorder [40].

In this study, to further investigate whether mTMEM16B induces Ca^{2+}-activated Cl^- currents not only in Axolotl oocytes as reported by Schroeder et al. [51], but also in a mammalian cell line, and to examine in detail its functional characteristics, we expressed TMEM16B in HEK 293T cells and analyzed its electrophysiological properties both in the whole-cell and in the excised inside-out configuration.

These data will improve our knowledge about the still elusive molecular identity of Ca^{2+}-activated Cl^- channels and will contribute to understand the role of TMEM16B in physiological and pathophysiological processes.

Materials and methods

mTMEM16B transfection and electrophysiological recordings

Full-length mTMEM16B cDNA in pCMV-Sport6 mammalian expression plasmid was obtained from the RZPD (Berlin, Germany; clone identification: IRAVp968H1167D). mTMEM16B was transfected into HEK 293T cells by using FuGENE 6 reagent (Roche Applied Science, Mannheim, Germany). Cells were cotransfected with enhanced green fluorescent protein (EGFP) in pGFP (Clontech, Mountain View, CA, USA), and transfected cells were identified by EGFP fluorescence.

Electrophysiological recordings from HEK 293T cells expressing mTMEM16B were performed in the whole-cell or inside-out patch-clamp configurations. Patch pipettes

were made of borosilicate glass (WPI, Sarasota, FL, USA) with a PP-830 puller (Narishige, Tokyo, Japan). Currents were recorded with an Axopatch 1D amplifier controlled by Clampex 9 via a Digidata 1332A (Axon Instruments, Union City, CA, USA).

For current–voltage relations in the inside-out configuration, care was taken not to introduce an artificial rectification due to the inactivation of the channel. For this purpose, patches were pre-exposed to the test Ca^{2+} concentration for 500 ms at −100 mV to allow the current to partially inactivate. At 100 μM Ca^{2+}, 15±6% (n=8) of the current inactivated in 500 ms. After the pre-exposition at the test Ca^{2+} concentration, a double voltage ramp from −100 to +100 mV and back to −100 mV was applied at 1 mV/ms. The two current–voltage relations were averaged, and leak currents measured with the same ramp protocol in Ca^{2+}-free solutions were subtracted.

Data were low-pass-filtered at 4 kHz and sampled at 10 kHz.

To estimate the single-channel amplitude, mean current and current variance were calculated from patches exposed to 1.5 μM Ca^{2+} or to 0 Ca^{2+} for 2 s at the holding potential of −50 mV. To avoid possible errors resulting from baseline drift, mean current and current variance were determined during 20 ms intervals. Values obtained from recordings in 0 Ca^{2+} were subtracted from those at 1.5 μM Ca^{2+}. The single-channel amplitude was estimated from the ratio between current variance and mean current.

Experiments were performed at room temperature (20–22°C). The bath was grounded via a 3-M KCl agar bridge connected to a Ag/AgCl reference electrode. Rapid solution exchange was achieved by transferring the excised membrane patch across the interface between neighboring solutions' streams using the perfusion Fast-Step SF-77B (Warner Instrument Corp., USA). Control experiments in nontransfected and only EGFP-transfected cells did not show any significant Ca^{2+}-activated current (data not shown). For flash photolysis of caged Ca^{2+}, flashes of ultraviolet light were delivered from a mercury lamp through an objective ×40 (NA 0.60, Olympus). The duration of light flashes was controlled by a mechanical shutter (Uniblitz, Vincent Associates, USA).

Ionic solutions

For whole-cell recordings, the standard extracellular solution contained (in mM): 140 NaCl, 5 KCl, 2 $CaCl_2$, 1 $MgCl_2$, and 10 Hepes, pH 7.4. The pipette solution contained (in mM): 140 cholineCl, 10 Hepes, and 10 HEDTA, pH 7.2, and no added Ca^{2+} for the nominally 0 Ca^{2+} solution, 3.209 or 8.263 mM $CaCl_2$ to obtain 1.5 or 13 μM free Ca^{2+}, respectively [41]. The intracellular recording solution for the photorelease of caged Ca^{2+} contained (in mM): 3 DMNP-EDTA, 1.5 $CaCl_2$, 140 CsCl, and 10 Hepes, pH 7.2. DMNP-EDTA was purchased from Molecular Probes-Invitrogen (OR, USA), and $CaCl_2$ was adjusted with a 0.1-M standard solution from Fluka (Germany). The caged compound was allowed to diffuse freely from the patch pipette into the cytoplasm of HEK 293T cells for at least 3 min after establishment of the whole-cell configuration.

For inside-out recordings, the standard solution in the patch pipette contained (in mM): 140 NaCl, 10 HEDTA, and 10 Hepes, pH 7.2. In experiments for Ca^{2+} dose–response relations, NaCl was replaced with LiCl to inhibit the possible activity of Na^+/Ca^{2+} exchangers in HEK 293T cell membranes. The bathing solution at the intracellular side of the patch contained (in mM): 140 NaCl or LiCl, 10 HEDTA, and 10 Hepes, pH 7.2, and no added Ca^{2+} for the nominally 0 Ca^{2+} solution, or various added Ca^{2+} concentrations, as calculated with the program WinMAXC (C. Patton), to obtain free Ca^{2+} in the range between 1.5 and 100 μM [41]. The free Ca^{2+} concentrations were experimentally determined by Fura-4F (Molecular Probes-Invitrogen) measurements by using an LS-50B luminescence spectrophotometer (PerkinElmer, Wellesley, MA, USA). For permeability experiments, Cl^- was substituted with other anions by replacing NaCl on an equimolar basis with NaX, where X is the substituted anion, or NaCl was replaced with equimolar choline chloride. Liquid junction potentials were calculated using pClampex software and applied voltages were corrected off-line for the following values (in mV): +2.1 for Cl, +0.1 for isothiocyanate (SCN), +2.4 for Br, +2.1 for I, +1.1 for NO_3, −3.6 for methanesulfonate (MeS), +6.0 for gluconate, +4.5 for choline).

For activation by various divalent cations, the solution at the intracellular side of the patch contained (in mM): 1 EGTA and 2 $CaCl_2$, or 1.09 $SrCl_2$, or 1.09 $BaCl_2$, or 1.03 $MgCl_2$, to obtain 1 mM of each free divalent cation, as calculated with the program WinMAXC (C. Patton). Niflumic, flufenamic, and mefenamic acids and 5-Nitro-2-(3-phenylpropylamino)benzoic acid (NPPB) were prepared in dimethyl sulfoxide (DMSO) at 200 mM (or 81 mM for NPPB) as stock solutions and diluted to the final concentration in the bathing solution (DMSO alone did not alter the mTMEM16B currents); 4-acetamido-4[prime]-isothiocyanato-stilben-2,2[prime]-disulfonate (SITS) and 4,4′-diisothiocyanatostilbene-2,2′-disulfonic acid (DIDS) were directly dissolved in the bathing solution. MgATP (2 mM), Na_3VO_4 (0.1 mM), dithiothreitol (DTT; 10 mM), calmodulin (500 nM), cyclic adenosine monophosphate (cAMP; 1 mM) were directly dissolved in the bathing solution. PIP_3 diC8 (Echelon Biosciences, Salt Lake City, UT, USA) was dissolved in water at 1 mg/ml after sonication for 5 min and diluted to 10 μM in the bathing solution. Histamine was dissolved in water at 100 mM and

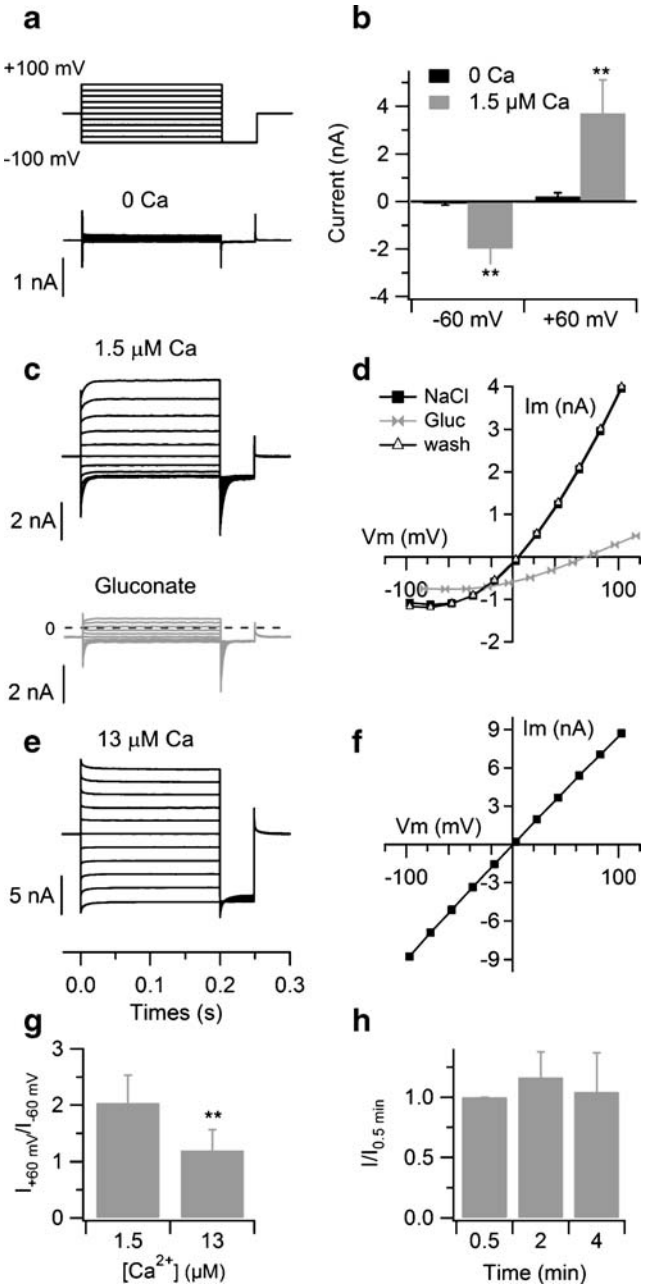

Fig. 1 Whole-cell Ca^{2+}-activated currents induced by mTMEM16B transfection in HEK 293T cells. Whole-cell voltage-clamp recordings obtained with a pipette solution containing nominally 0 Ca^{2+} (**a**), 1.5 μM free Ca^{2+} (**c**), or 13 μM free Ca^{2+} (**e**). The time scale plotted in **e** is the same also for **a** and **c.** Voltage steps of 200 ms duration were given from a holding potential of 0 mV to voltages between −100 and +100 mV in 20 mV steps followed by a step to −100 mV. In some traces, capacitative transients were trimmed. **c** Currents were activated by 1.5 μM Ca^{2+} and the same cell was exposed to a solution containing NaCl (*black traces at the top*) or to Na-gluconate (*gray traces at the bottom*). **b** Mean current amplitudes measured at the end of the voltage steps at −60 mV or at +60 mV with intracellular pipette solution containing nominally 0 (*black bar*; n=6) or 1.5 μM free Ca^{2+} (*gray bar*; n=7). Data are shown as mean values ± standard deviations (**p<0.01, unpaired t test). **d** Current–voltage relations activated by 1.5 μM Ca^{2+} measured at the end of the voltage steps from the cell shown in **c**. *Black squares* represent control data in symmetrical Cl^- and are superimposed to *white triangles*, representing data after wash out from the gluconate solution (*gray symbols*). **e** Currents activated by 13 μM Ca^{2+}. **f** Current–voltage relation activated by 13 μM Ca^{2+} measured at the end of the voltage steps from the cell shown in **e**. **g** Ratios between currents measured at +60 and at −60 mV at 1.5 and 13 μM Ca^{2+} (n= 5–9, **p<0.01, unpaired t test). **h** Average values of relative current amplitudes at −60 mV measured 0.5, 1, or 4 min after reaching the whole configuration (n=5–7)

diluted in Ringer solution. All chemicals, unless otherwise stated, were purchased from Sigma.

Statistical analysis

Data are presented as mean ± standard deviation, with n indicating the number of cells or of excised patches. Statistical significance was determined using paired or unpaired t tests, or ANOVA, as appropriate. When a statistically significant difference was determined with ANOVA, a post hoc Tukey test was done to evaluate which data groups showed significant differences. P values <0.05 were considered significant. Data analysis and figures were made with Igor software (Wavemetrics, Lake Oswego, OR, USA).

Results

Ca^{2+} activation of a Cl^- current induced by mTMEM16B in mammalian HEK 293T cells

We transfected mTMEM16B in HEK 293T cells and measured the current in the whole-cell configuration increasing the intracellular Ca^{2+} concentration in several ways.

In a first set of experiments, cells were dialyzed with intracellular solutions containing various amounts of Ca^{2+}. Figure 1 shows that 1.5 μM Ca^{2+} generated a large current (Fig. 1c), while the current in nominally 0 Ca^{2+} was negligible (Fig. 1a), showing that Ca^{2+} ions activate a current in HEK 293T cells transfected with mTMEM16B (Fig. 1b). To examine whether the current was carried by Cl^-, we reduced the extracellular Cl^- concentration by replacing NaCl with Na-gluconate (Fig. 1c, d) and measured an average shift of reversal potential of +44±9 mV (n=14). The reversal potential in the low Cl^- solution shifted toward the value expected for Cl^- channels in our ionic conditions, although the expected shift for a perfectly Cl^- selective channel in these ionic conditions would be of +64 mV. However, the difference could be ascribed to a partial permeation of gluconate and/or of Na^+, as previously shown for other anion channels [15, 46].

In the presence of 1.5 μM Ca^{2+}, the current–voltage relation in symmetrical Cl^- solutions, measured at the end of

the voltage steps (Fig. 1d), clearly showed a pronounced outward rectification. When the intracellular Ca^{2+} concentration was increased to 13 μM (Fig. 1e), the rectification properties changed and the current–voltage relation became linear (Fig. 1f). The average ratio between the current measured at the end of voltage pulses at +60 and −60 mV from several cells (Fig. 1g) shows that the current–voltage relations in symmetrical Cl^- solutions were Ca^{2+}-dependent. A change in the rectification properties from an outward to a linear rectification increasing intracellular Ca^{2+} concentrations is a well-known characteristic of some Ca^{2+}-activated Cl^- channels [1, 9, 26, 29].

We observed that, in the presence of 1.5 μM Ca^{2+}, current activation in response to voltage steps was time-dependent. Indeed, depolarizing voltage steps (from +40 to +100 mV) elicited outward currents with two components: an instantaneous current followed by an outward relaxation (Fig. 1c). Hyperpolarizing voltage steps (from −40 to −100 mV) induced inward currents also consisting of two components: an instantaneous current followed by a relaxation toward less negative values (Fig. 1c). Both outward and inward relaxations were well fitted by single exponentials (data not shown). At +100 mV, the time constant of the outward relaxation was 4.4±0.6 ms (n=7), while at −100 mV, the time constant of the inward relaxation was 7.1±0.9 ms (n=7), and the two means were significantly different ($p<$ 0.01). In these experiments, the instantaneous current elicited by a given voltage step is carried by channels open at the holding potential of 0 mV, while the development of the current relaxations is due to the change in open probability at the given voltage step; therefore, the analysis of current relaxations indicated that, in the presence of 1.5 μM Ca^{2+}, the open probability increased at depolarized potentials, while it decreased at hyperpolarized potentials. When the intracellular Ca^{2+} concentration was raised to 13 μM (Fig. 1e), the relaxations were not present anymore, indicating that the channel open probability was already the same at every potential. These data show that the opening of the mTMEM16B-induced currents is regulated by both Ca^{2+} and voltage, as previously observed in some native Ca^{2+}-activated Cl^- channels [1, 9].

To examine if whole-cell currents exhibited a rundown, we compared the current amplitudes at the end of a voltage step to −60 mV applied at different times after reaching the whole-cell configuration. On average, the relative amplitude of the current at 4 min was 104±33% (n=7) of the control value measured at 0.5 min after obtaining the whole-cell configuration (Fig. 1h). These results indicate that, during the tested time interval, whole-cell recordings did not show any significant rundown, although we cannot exclude the possibility that rundown had already occurred before the beginning of our recordings. In some cells, the current maintained its initial amplitude (at 0.5 min) for up to 30 min.

To determine the pharmacological profile of mTMEM16B in the whole-cell configuration, we measured the extracellular blockage properties of several molecules that are commonly used as blockers of Ca^{2+}-activated Cl^- currents (for reviews, see [10, 13]). As shown in Fig. 2a–d, NFA, NPPB, SITS, and DIDS, produced a partial block of both inward and outward currents activated by 1.5 μM Ca^{2+}. The blockage by NFA, SITS, and DIDS was completely reversible, while NPPB inhibition was only partially reversible. The percentage of current inhibition at −60 mV (+60 mV) was 69% (81%) for NFA, 65% (67%) for NPPB, 70% (82%) for SITS, and 62% (79%) for DIDS.

In a second set of experiments, instead of dialyzing the cell with Ca^{2+} diffusing from the patch pipette, we elicited a transient increase in the intracellular Ca^{2+} concentration by coexpressing mTMEM16B with the histamine receptor subtype 1 (H1R) and activating the receptor with histamine. Figure 3a shows that a large current was activated at the holding potential of −50 mV by the application of 100 μM histamine. The current–voltage relation obtained with a voltage ramp from −100 to +100 mV (Fig. 3b) was very similar to that measured with 1.5 μM Ca^{2+} in pipette (Fig. 1e). No significant currents were activated by histamine in control experiments with nontransfected cells or with cells transfected with H1R alone (Fig. 3c).

To further investigate whether the current induced by mTMEM16B is directly activated by Ca^{2+}, we photoreleased Ca^{2+} inside the cell. In these experiments, the patch pipette contained caged Ca^{2+} and we measured the current in response to an increase of intracellular Ca^{2+} obtained with a flash of ultraviolet light, while the holding potential was −50 mV. Figure 4 shows that currents were rapidly generated upon photorelease of Ca^{2+}. Control experiments demonstrated that no Ca^{2+}-induced currents were induced in nontransfected HEK 293T cells (data not shown). Currents of increasing amplitudes were measured when intracellular Ca^{2+} concentration was increased by lengthening the duration of the ultraviolet flash photoreleasing Ca^{2+} (Fig. 4a). The normalized currents as a function of flash duration were well fitted by a Hill equation (Fig. 4b). Thus, the experiments shown in Fig. 4 indicate that Ca^{2+} directly activates a current induced by mTMEM16B in HEK 293T cells.

Ca^{2+} activation of the mTMEM16B-induced current in excised patches

To further investigate Ca^{2+} activation of mTMEM16B-induced current, we obtained a precise control of the Ca^{2+} concentration by using the patch-clamp technique in the excised inside-out configuration from HEK 293T cells expressing mTMEM16B. In these experiments, we used a perfusion system that allows a fast change of solution. The

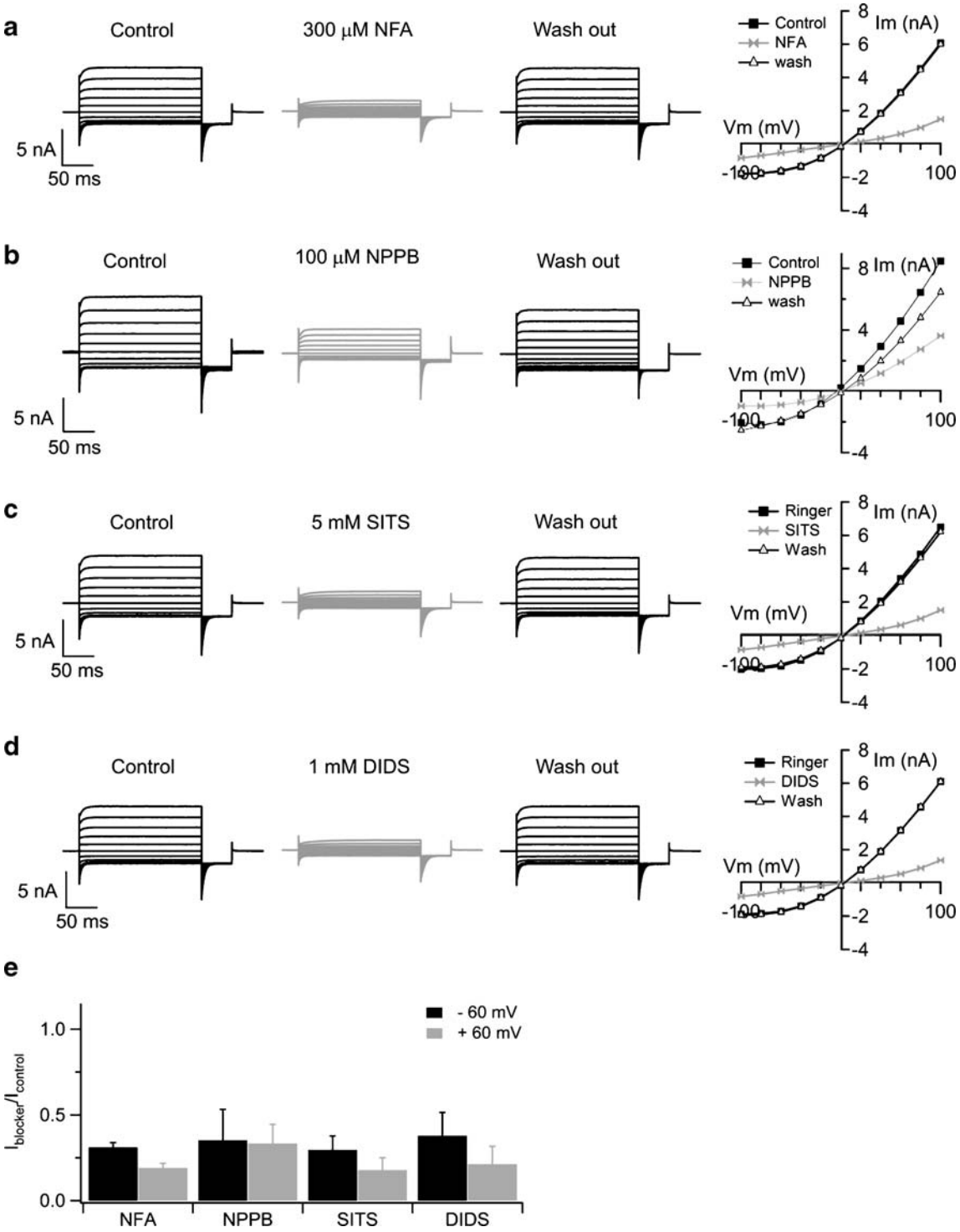

Fig. 2 Extracellular blockage by some Cl^- channel blockers of whole-cell Ca^{2+}-activated currents induced by mTMEM16B transfection in HEK 293T cells. Whole-cell voltage-clamp recordings obtained with a pipette solution containing 1.5 μM free Ca^{2+} in symmetrical Cl^- solutions. Voltage steps of 200 ms duration were given from a holding potential of 0 mV to voltages between −100 and +100 mV in 20 mV steps followed by a step to −100 mV. In some traces, capacitative transients were trimmed. **a** 300 μM NFA, **b** 100 μM NPPB, **c** 5 mM SITS, **d** 1 mM DIDS. Current recordings were obtained at control, 2 min after application of the indicated blockers, and 2 min after the removal of blockers (wash out). For NPPB, a complete wash out was not obtained up to 10 min after blocker removal. *Panels on the right* are current–voltage relations measured at the end of the voltage steps. **e** Average ratios between currents measured at −60 mV (*black bars*) or at +60 mV (*gray bars*) in the presence and in the absence of the indicated blockers (n=3–7; p<0.05)

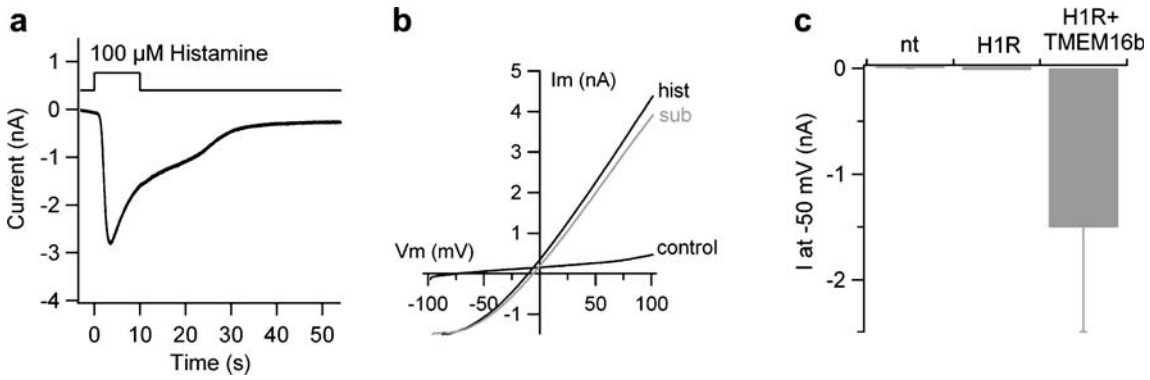

Fig. 3 Whole-cell currents activated by histamine in HEK 293T cells transfected with mTMEM16B and the histamine receptor H1R. **a** Current activated by 100 µM histamine applied for the time indicated in the upper trace. The holding potential was −50 mV. **b** Currents evoked by voltage ramps from −100 to +100 mV in the absence of histamine (control) or 4 s after the application of 100 µM histamine. The *gray trace* (*sub*) was obtained by subtracting the control trace from the trace measured in the presence of histamine. **c** Mean current amplitudes at −50 mV measured after application of 100 µM histamine from nontransfected cells (*nt*; n=6), and cells transfected with H1R (n=11) alone, or with H1R and TMEM16B (n=5), as indicated

excised membrane patch was held in front of a glass pipe where a nominally 0 Ca^{2+} solution was continuously flowing, and Ca^{2+} was applied by rapidly moving the patch position in front of the adjacent pipe, where a Ca^{2+}-containing solution was flowing.

Figure 5a shows currents activated by the exposure of the cytoplasmic side of the patch to 100 µM Ca^{2+} for 2 s at the holding potential of −50 mV. Ca^{2+}-activated currents showed two time-dependent characteristics. Upon application of 100 µM Ca^{2+}, the current rapidly increased reaching a peak and then slowly decreased in the presence of the constant Ca^{2+} concentration, a process that we call here inactivation and that will be described in more detail below (Fig. 6). The other time-dependent behavior was an irreversible decrease in the current amplitude with time, a process that we define as rundown (Fig. 5a). To estimate the amount of rundown, we measured the current at −50 mV at the beginning of the experiment exposing the patch for 2 s to 100 µM Ca^{2+}, then the membrane patch was kept in the nominally 0 Ca^{2+} solution until the following 100 µM Ca^{2+} application. Subsequent exposures to Ca^{2+} produced currents of decreasing amplitudes. The time course of the rundown was fast in the first minutes after patch excision and slowed down with time, and sometimes the current reached a stationary current level (Fig. 5b), although there was a great variability between membrane patches. The average normalized current as a function of time could be fitted by a single exponential function with a time constant of 1.11 min (Fig. 5b). A similar rundown was also observed at positive voltages (data not shown). We attempted to revert the rundown by applying several agents that have been shown to sustain the activity of other channels in excised patches [44]. We tested adenosine triphosphate (ATP; to sustain the kinases activity), DTT (to maintain a reducing environment), calmodulin, PIP_3 (a cofactor of many ion channels [7, 31, 44]), cAMP, and Na_3VO_4 (to inhibit tyrosine and alkaline phosphatases), but none of these appeared to significantly alter the rundown (Fig. 5c).

Most of the experiments presented in this study were performed after the rapid phase of rundown when the current reached an almost steady-state value.

The other time-dependent behavior, inactivation, is analyzed in more detail in Fig. 6. In contrast to rundown, inactivation appeared to be largely reversible. Indeed, when experiments were performed after the rapid phase of rundown, at the almost steady-state level, current inactivation was found to be largely reversible after removal of 100 µM Ca^{2+} for at least 1 min. Figure 6a shows superimposed current traces at −50 mV measured at 5 and at 6 min after patch excision: the peak current at 6 min

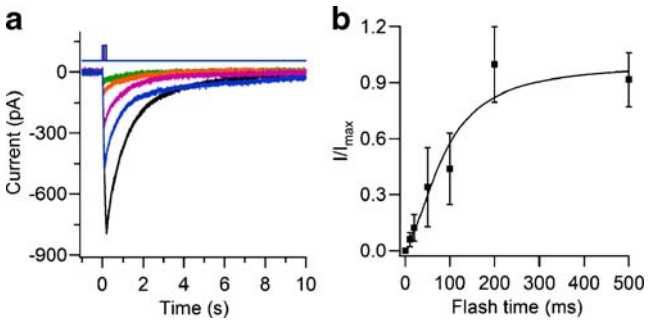

Fig. 4 Whole-cell currents activated by photorelease of caged Ca^{2+}. **a** Caged Ca^{2+} (DMNP-EDTA) diffused into the cell from the patch pipette and ultraviolet flashes of increasing duration were applied to the cell to photorelease Ca^{2+}. The holding potential was −50 mV. **b** Average currents normalized to their maximal value were plotted versus flash duration and fitted to the Hill equation: $I/I_{max} = d^{n_H} \Big/ \left(d^{n_H} + d_{1/2}^{n_H}\right)$, where d is the flash duration, $d_{1/2}$ the flash duration producing half of the maximal current, and n_H is the Hill coefficient. The value for $d_{1/2}$ was 88 ms and n_H was 1.8 (n=6)

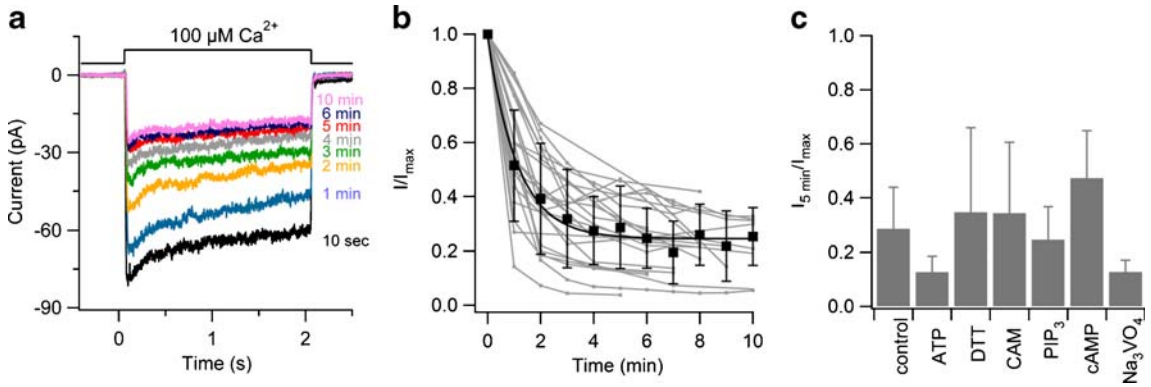

Fig. 5 Rundown of the mTMEM16B-mediated current in excised inside-out membrane patches. **a** An inside-out membrane patch was excised from HEK 293T cells transfected with mTMEM16B and the cytoplasmic side was exposed to 100 μM Ca^{2+} at the time indicated in the *upper trace*. The holding potential was −50 mV. The *number next to each trace* indicates the initial time of Ca^{2+} application after patch excision. Rundown: repetitive applications of Ca^{2+} produced a current of decreasing amplitude. **b** The ratios between the peak current at various times after patch excision and the maximal current measured at patch excision were plotted against the time after patch excision for several patches (*gray dots and lines*). In *black*, the mean from different patches with standard deviation (n=5–32); the *line* was the best fit to a single exponential with a time constant of 1.11 min. **c** Various compounds, as indicated in the figure, were tested for their ability to prevent the rundown, but none of them produced a significant change in rundown. Ratios between current amplitudes measured 5 min after patch excision and the maximal current (n=3–10). Average values for each compound were not significantly different from control (ANOVA, F=1.85, p=0.209)

almost reached the peak value previously measured at 5 min, indicating that the inactivation process is Ca^{2+}-dependent and reversible.

To analyze if inactivation was voltage-dependent, we measured currents activated at −50 or +50 mV. In the presence of the constant 100-μM Ca^{2+} concentration, the current at −50 mV decreased with time, while the current at +50 mV had a stationary value (Fig. 6b). On average, at −50 mV, the current measured after 1 s from the beginning of Ca^{2+} exposure was reduced of 28±6% (n=13) compared to the peak current, whereas at +50 mV, the current reduction was only 1.4±0.9% (n=4; black bar in Fig. 6d), indicating that inactivation is a voltage-dependent process.

To investigate the Ca^{2+} dependence of inactivation, we measured currents activated by various Ca^{2+} concentrations at the holding potential of −50 mV. The current measured after 1 s from the beginning of Ca^{2+} exposure was reduced to 15±5% for 3.8 μM Ca^{2+} (n=8) compared to the peak current, and the reduction was significantly different from the value of 28±6% (n=13) for 100 μM Ca^{2+} (Fig. 6c, d). These results further indicate that inactivation is a Ca^{2+}-dependent process.

To determine whether inactivation was dependent on how much rundown has occurred, we analyzed current inactivation during the rundown. Figure 6e shows normalized currents measured at the beginning of the experiment (10 s after patch excision) and at the almost steady state (5 min after patch excision) from the experiment shown in Fig. 5a. The superimposition of the two normalized current traces indicates that the amount of current decrease was independent of rundown, as further illustrated in Fig. 6f, showing that the average amount of inactivation measured at different times from patch excision did not significantly change.

We also investigated whether the inactivation process could be modified by the application of the agents used in the attempt to revert rundown and we did not find any significant change (data not shown).

Next, we analyzed the Ca^{2+} activation kinetics of the mTMEM16b-mediated current by measuring the rise time of the current response to the application of various Ca^{2+} concentrations in excised inside-out patches. First, we estimated the time necessary for the solution exchange in our perfusion system by measuring the current variation at 0 mV when a patch electrode was moved from Ringer to 1 M KCl solution (Fig. 7a). The time required for the solution exchange was 3±1 ms (n=12). The application of 100 μM Ca^{2+} at the cytoplasmic side of a patch at the holding potential of −50 mV activated a current (Fig. 7b) with a rise time of 36±15 ms (n=16). The rise time of the current response became slower when Ca^{2+} concentration was lowered, with average values of 85±20 ms (n=5) at 3.8 μM Ca^{2+} and 134±66 ms (n=4) at 1.5 μM Ca^{2} (Fig. 7b, c).

Finally, we attempted to directly measure the amplitude of single-channel events in membrane patches containing many channels by decreasing the channel open probability using low Ca^{2+} concentrations. Currents were activated by 1.5 μM Ca^{2+} at the holding potential of −50 mV for 2 s. Since we could not distinguish any single-channel event from the background noise, we estimated the single-channel amplitude by calculating the ratio between variance and mean of macroscopic currents at 1.5 μM Ca^{2+} [15]. The estimated single-channel amplitude at −50 mV was 0.06±

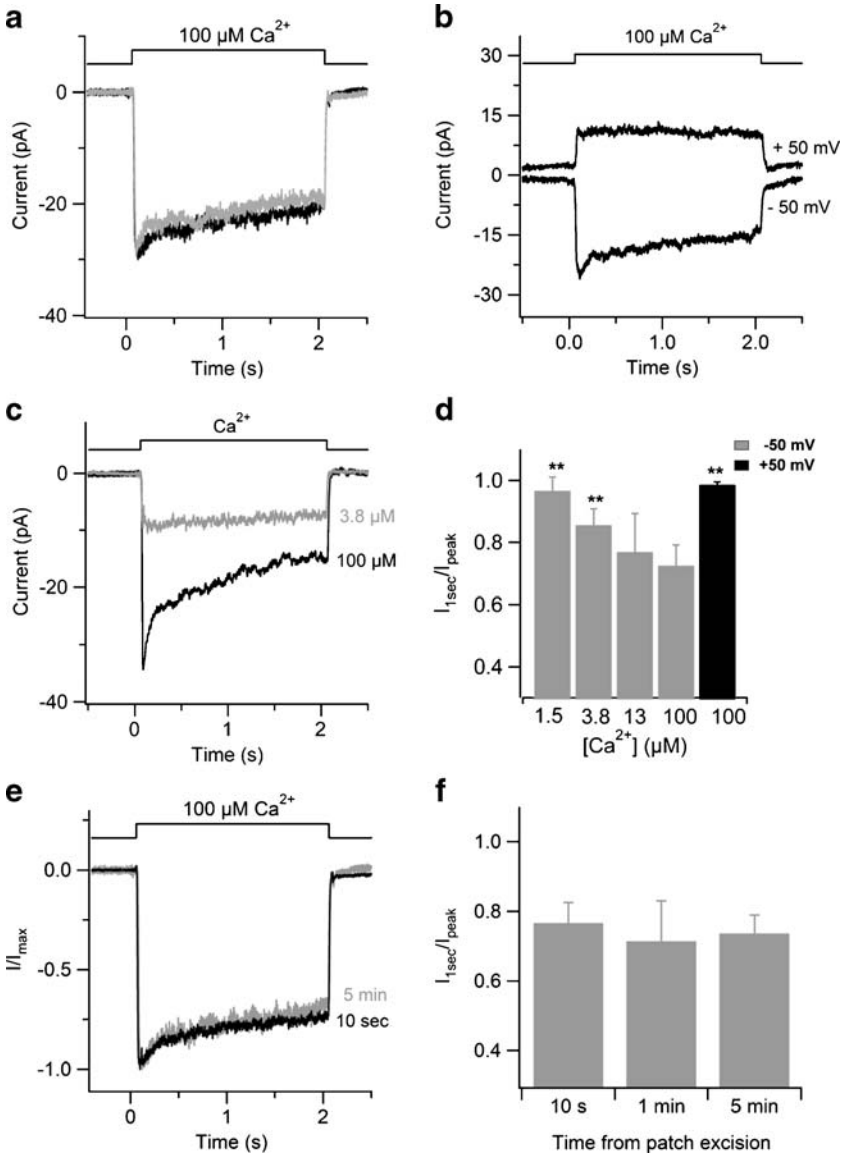

Fig. 6 Ca^{2+}- and voltage-dependent inactivation of the mTMEM16B-mediated current in excised inside-out membrane patches. **a** An inside-out membrane patch was excised from HEK 293T cells transfected with mTMEM16B and the cytoplasmic side was exposed to 100 μM Ca^{2+} at the time indicated in the *upper trace*. The holding potential was −50 mV. Upon application of 100 μM Ca^{2+}, the current increased reaching a peak and then decreased in the presence of the constant Ca^{2+} concentration (inactivation). The inactivation process was largely reversible: the *black* and the *gray traces* are the responses to 100 μM Ca^{2+} measured, respectively, at 5 or 6 min after patch excision, from the experiment shown in Fig. 5a. **b** Inactivation was voltage-dependent. Currents activated by 100 μM Ca^{2+} at −50 mV or +50 mV after 3 or 4 min from patch excision, respectively. Current traces were from the same patch. The current at +50 mV was stationary (see also **d**). **c** Inactivation was Ca^{2+}-dependent. Currents activated by 100 μM (*black trace*) or 3.8 μM (*gray trace*) Ca^{2+} at −50 mV in the same patch showed different amounts of inactivation. **d** Mean ratios from several patches between the current measured 1 s after application of the indicated Ca^{2+} concentrations and the current measured at the peak, at −50 mV (*gray bars*) or at +50 mV (*black bar*) (n=4–13). Some mean current ratios were significantly different compared to the average value measured with 100 μM Ca^{2+} at −50 mV (**p<0.01; ANOVA, F=18.44, $p=3.1\times10^{-8}$ followed by Tukey test). **e** Currents measured at 10 s and at 5 min after patch excision, from the experiment shown in Fig. 5a, were normalized to their peak current and plotted as a function of time. **f** Mean ratios from several patches between the current measured 1 s after application of 100 μM Ca^{2+} and the current measured at the peak (n=5–7, ANOVA, F=3.68, p=0.59) at 10 s, 1 min, or 5 min after patch excision

0.02 pA (n=4), and the corresponding conductance was 1.2 pS, in the range of values expected for low conductance native Ca^{2+}-activated Cl^- channels ([16, 45, 47], for reviews, see [10, 13]).

The Ca^{2+}-activated current is carried by Cl^-

To investigate if the Ca^{2+}-activated current observed in inside-out patches is a Cl^- current, we examined whether it

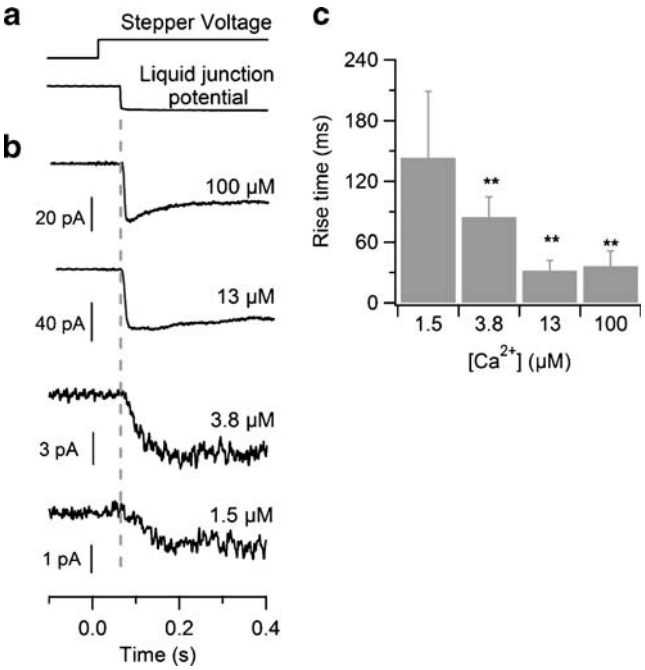

Fig. 7 Activation by Ca^{2+} of the mTMEM16B-mediated current in excised inside-out membrane patches. **a** Time course of the solution exchange. The *top trace* shows the voltage command of the stepper motor moving glass pipes in which different solutions were flowing. The *bottom trace* shows the time course of the solution exchange measured by moving a patch electrode held in front of a pipe in which a Ringer solution was flowing, to a pipe in which 1 M KCl solution was flowing. The delay between the voltage command and the beginning of the junction potential change was about 50 ms and was caused by the delay and by the speed of the mechanical movement bringing the different pipes in front of the patch electrode. The rise time of the solution exchange, defined as the time interval between the onset of the current change to the final current value, was about 3 ms. **b** mTMEM16B currents were recorded upon switching from a nominally 0 Ca^{2+} solution to the indicated Ca^{2+} concentrations. The rise time was faster for higher Ca^{2+} (100 and 13 µM) than for lower Ca^{2+} concentrations. Each recording was from a different patch. **c** Average values for the rise time at various Ca^{2+} concentrations (n=4–16, $^{**}p<0.01$; ANOVA, F=19.6, $p=4.8\times10^{-7}$ followed by Tukey test)

was reduced by typical blockers, such as niflumic acid, and we measured the reversal potential when Cl^- was replaced with other anions.

We examined the pharmacological profile of mTMEM16B at the cytoplasmic side by measuring the intracellular blockage properties of several blockers of Ca^{2+}-activated Cl^- currents. Figure 8a shows that the current activated by 100 µM Ca^{2+} was rapidly blocked by the application of 300 µM NFA to the intracellular side, and the blockage was reversible. To further examine the voltage dependence of the block, currents were activated using voltage ramps from −100 to +100 mV, and Fig. 8b illustrates that 300 µM NFA blocked the current in a voltage-independent manner. Two other fenamates, flufenamic and mefenamic acids, as well as NPPB and SITS, only partially blocked the current, whereas DIDS did not have any blocking effect at the intracellular side (Fig. 8c). The percentage of inhibition at −50 mV was 60% for FA, 20% for MFA, 19% for NPPB, 20% for SITS, and 0% for DIDS (Fig. 8c).

To determine the anion selectivity of the Ca^{2+}-activated current, we replaced NaCl in the bathing solution with NaI, NaBr, $NaNO_3$, NaIsothiocyanate (NaSCN), or NaMethanesulfonate (NaMeS) and measured the shift in reversal potential (Fig. 9). We could not test the permeability to fluoride because fluoride ions form an insoluble salt with calcium ions that are necessary to activate the channels. Currents were activated by 100 µM Ca^{2+} using voltage ramps from −100 to +100 mV. Replacement of Cl^- with MeS shifted the reversal potential from near zero in symmetrical Cl^- to more negative values, as expected for Cl^- selective channels in our experimental conditions, showing that Ca^{2+}-activated currents were Cl^- selective. Relative permeability ratios (P_X/P_{Cl}) calculated with the Goldman–Hodgkin–Katz relation from measured reversal potentials were SCN (12.8) > I (4.9) > NO_3 (3.7) > Br (2.1) > Cl (1.0) > MeS (0.1) (Fig. 9b).

Furthermore, since some anion channels are also permeable to cations [46, 54], we determined the relative Na^+ permeability replacing NaCl with choline chloride and found that P_{Na}/P_{Cl} was 0.23±0.07 (n=3).

These experiments show that the Ca^{2+}-activated current is indeed mainly carried by anions.

Ca^{2+} sensitivity and current–voltage relations

To examine the dependence of the mTMEM16B-induced current on the intracellular Ca^{2+} concentration, dose–response relations were obtained in excised inside-out patches by activating currents with various Ca^{2+} concentrations. Experiments were performed after the rapid phase of rundown when the current reached an almost steady-state value (Fig. 5). To take into account a remaining slow phase of the rundown that was present in some membrane patches, currents at each test Ca^{2+} concentration were normalized to the average current activated by 100 µM Ca^{2+} before and after the test Ca^{2+} concentration. Figure 10a–c illustrates the results of a representative dose–response experiment. Currents at each Ca^{2+} concentration were measured using voltage ramps from −100 to +100 mV. Normalized currents measured at +50 and at −50 mV were plotted in Fig. 10d versus Ca^{2+} concentration and fitted by the Hill equation: $I/I_{max} = c^{n_H} \Big/ \left(c^{n_H} + K_{1/2}^{n_H}\right)$, where c is the Ca^{2+} concentration, $K_{1/2}$ the Ca^{2+} concentration producing half-maximal current activation, and n_H is the Hill coefficient. The Ca^{2+} sensitivity was slightly voltage-dependent with a $K_{1/2}$ of 4.9 µM at −50 mV and 3.3 µM at +50 mV (Fig. 10d). The Hill coefficient was 2.5 at −50 mV and 2.0 at +50 mV. At −60 mV, $K_{1/2}$ was 5.1 µM with n_H=2.1, while at +60 mV, $K_{1/2}$ was 4.0 µM with n_H=1.9.

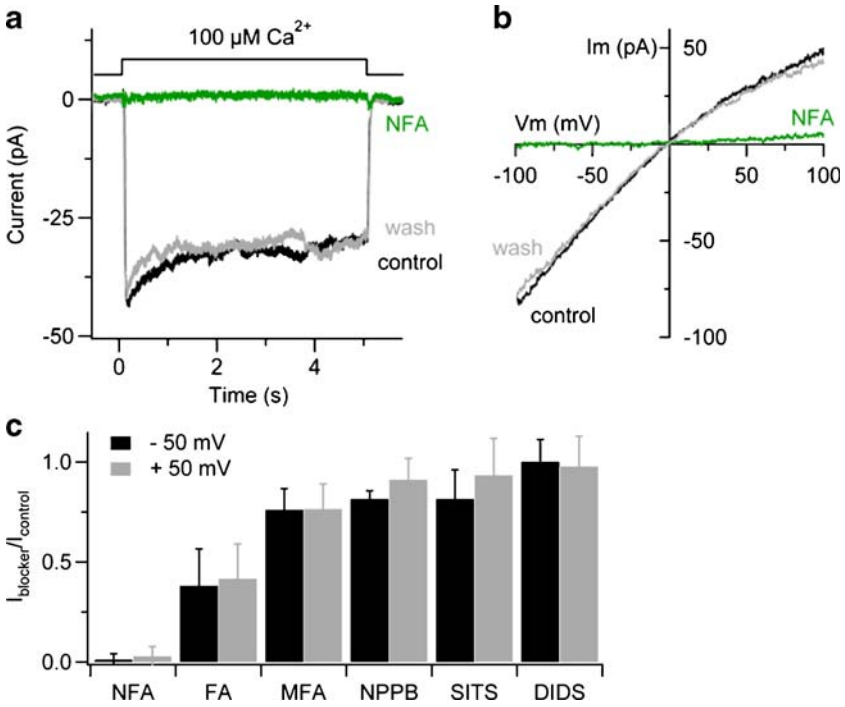

Fig. 8 Intracellular blockage by some Cl^- channel blockers of mTMEM16B-induced currents. **a** mTMEM16B currents were activated in inside-out patches by 100 µM Ca^{2+} at −50 mV or **b** with voltage ramps. In the same patch, bath application of 300 µM NFA rapidly and reversibly blocked the current. **c** Other compounds had smaller blocking effects. Ratios between currents measured in the presence and in the absence of 300 µM NFA, FA, or MFA; 100 µM NPPB; 5 mM SITS; 1 mM DIDS (n=5–9; p<0.05 for all compounds except for DIDS)

Since some Ca^{2+}-activated Cl^- channels are also activated by high concentrations of other divalent cations [38, 47], we tested whether mTMEM16B is activated by 1 mM Ba^{2+}, Sr^{2+}, and Mg^{2+}, using an experimental protocol similar to that described above for Ca^{2+} dose–response curves. Sr^{2+} efficiently activated a current (I_{Sr}/I_{Ca}=0.77±0.09, n=5), while Ba^{2+} only activated a small current (I_{Ba}/I_{Ca}=0.04±0.02, n=4), and no current was measured in the presence of Mg^{2+} (Fig. 11).

Furthermore, we observed that the current–voltage relations in symmetrical Cl^- solutions were Ca^{2+}-dependent. The current–voltage relation was outwardly rectifying at 1.5 µM Ca^2, linear at 3.8 µM Ca^{2+}, and inwardly rectifying at 13 and 100 µM Ca^{2+} (Fig. 12). A change in the rectification properties when intracellular Ca^{2+} concentrations vary is a well-known characteristic of some Ca^{2+}-activated Cl^- channels [1, 9, 26].

Discussion

Ca^{2+} activation

In this study, we have shown that mTMEM16B generates Ca^{2+}-activated Cl^- currents when expressed in the mammalian cell line HEK 293T. We measured currents both in the whole-cell and in the inside-out membrane patch configurations of the patch-clamp technique. In the whole-cell configuration, the intracellular Ca^{2+} concentration was increased in several ways: with a constant high Ca^{2+} concentration in the patch pipette, by releasing Ca^{2+} from intracellular stores through activation of a G-protein-coupled receptor (H1R), or by directly photoreleasing Ca^{2+} from caged Ca^{2+} inside the cell. In every type of experiment, we measured large Ca^{2+}-activated Cl^- currents (Figs. 1, 2, and 3).

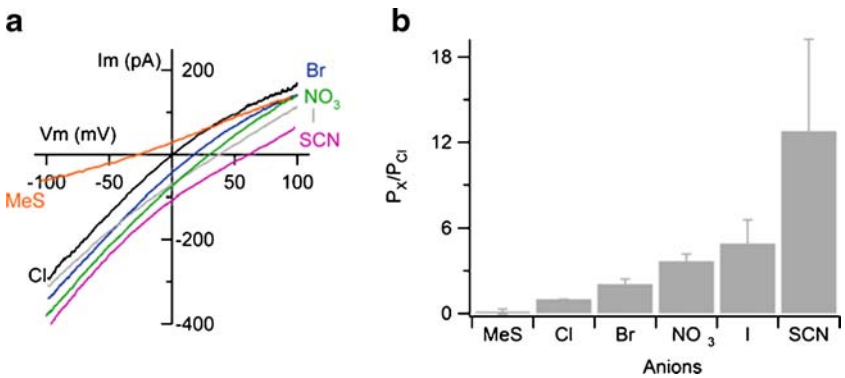

Fig. 9 Anion selectivity of the mTMEM16B-mediated current. **a** Current–voltage relations for mTMEM16B currents activated by 100 µM Ca^{2+} in an inside-out membrane patch, obtained from a ramp protocol. Bath solutions contained 140 mM NaCl or the Na salt of other anions, as indicated. Current traces were from the same patch. **b** Relative permeability ratios (P_X/P_{Cl}) calculated with the Goldman–Hodgkin–Katz equation (n=6–7)

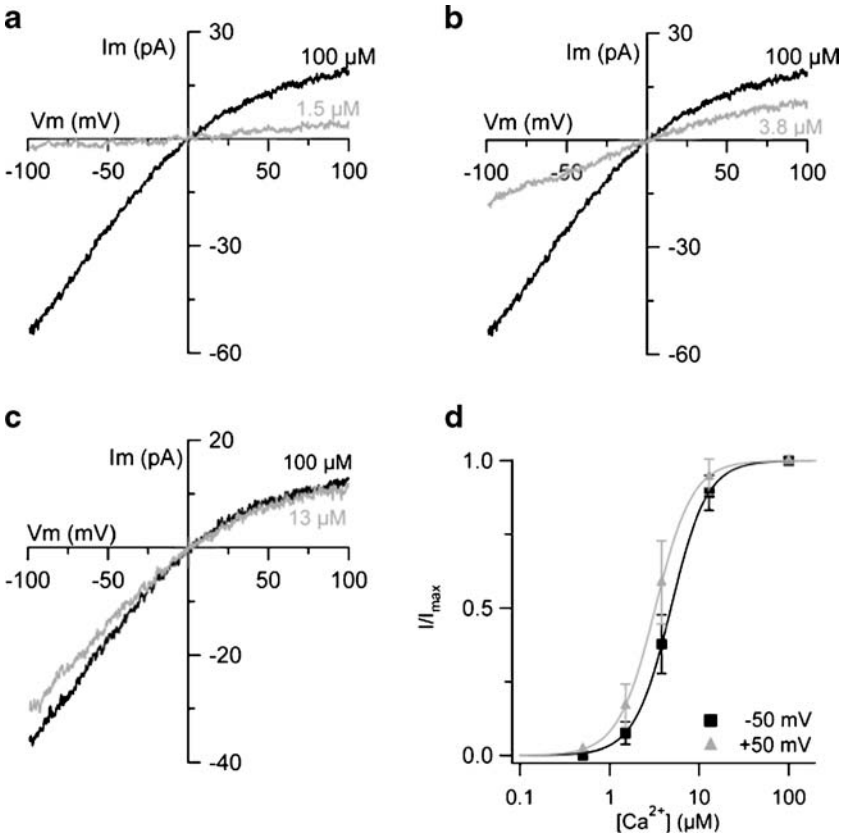

Fig. 10 Ca^{2+} sensitivity of mTMEM16B-mediated currents in inside-out membrane patches. An inside-out membrane patch was excised from HEK 293T cells transfected with mTMEM16B and the cytoplasmic side was exposed to 100 μM Ca^{2+} (*black traces*) or to **a** 1.5 μM Ca^{2+}, **b** 3.8 μM Ca^{2+}, and **c** 13 μM Ca^{2+}. *Black traces* are the average currents activated by 100 μM Ca^{2+} applied before and after the test Ca^{2+} concentration. Leakage currents measured in 0 Ca^{2+} were subtracted. Current traces were from the same patch. **d** Dose–response relations of activation by Ca^{2+} were obtained by normalized currents and fitted to the Hill equation. Currents at each test Ca^{2+} concentration were normalized to the average current measured in the presence of 100 μM Ca^{2+} before and after the test Ca^{2+} concentration. The Hill coefficient was 2.5 at −50 mV and 2.0 at +50 mV. Currents were half-maximal at 4.9 μM Ca^{2+} at −50 mV, and at 3.3 μM Ca^{2+} at +50 mV and these values were statistically different (n=6–7; p=0.02, unpaired t test)

These results further extend a previous report by Schroeder et al. [51], in which Ca^{2+}-activated Cl^- currents were induced by the expression of mTMEM16B in Axolotl oocyte. Since mTMEM16B produces Ca^{2+}-activated Cl^- currents in two very different expression systems, Axolotl oocytes and mammalian HEK 293T cells, it is likely that the currents originate from mTMEM16B rather than from upregulation of an endogenous chloride channel protein in the cell line, as what occurred for example for hCLCA1 [12]. Additional indications that mTMEM16B does form a Ca^{2+}-activated Cl^- channel arise from the many similarities with the properties of the TMEM16A channel and the native olfactory Ca^{2+}-activated Cl^- channel, as discussed later.

We extended the analysis of currents induced by mTMEM16B in HEK 293T cells performing experiments with the excised inside-out membrane patch configuration, which allows the rapid bath application of controlled Ca^{2+} concentrations, and also measured Ca^{2+}-activated Cl^- currents. These results, together with those in whole-cell showing rapid activation of channels by Ca^{2+} photorelease, indicate that mTMEM16B can be directly gated by Ca^{2+}. Moreover, we also observed that, after patch excision, mTMEM16B displays two interesting time-dependent behaviors: a decrease of current amplitude during the constant application of high Ca^{2+} concentrations at −50 mV (inactivation) and an irreversible rundown. The inactivation process was reversible, voltage-dependent, and Ca^{2+}-dependent, being more pronounced at hyperpolarized potentials and at high Ca^{2+} concentrations. The rundown of the current was irreversible and showed a fast current decline in the first minute after patch excision, reaching a relatively stationary value afterwards, indicating that some modulatory substrates may be lost after patch excision. In the attempt to determine the rundown mechanism, we added several compounds to the cytoplasmic side of the patch, but none of them was effective in reducing the rundown (Fig. 5c). Our results indicate that membrane-bound kinases and tyrosine and alkaline phosphatases are not involved in rundown because ATP and Na_3VO_4

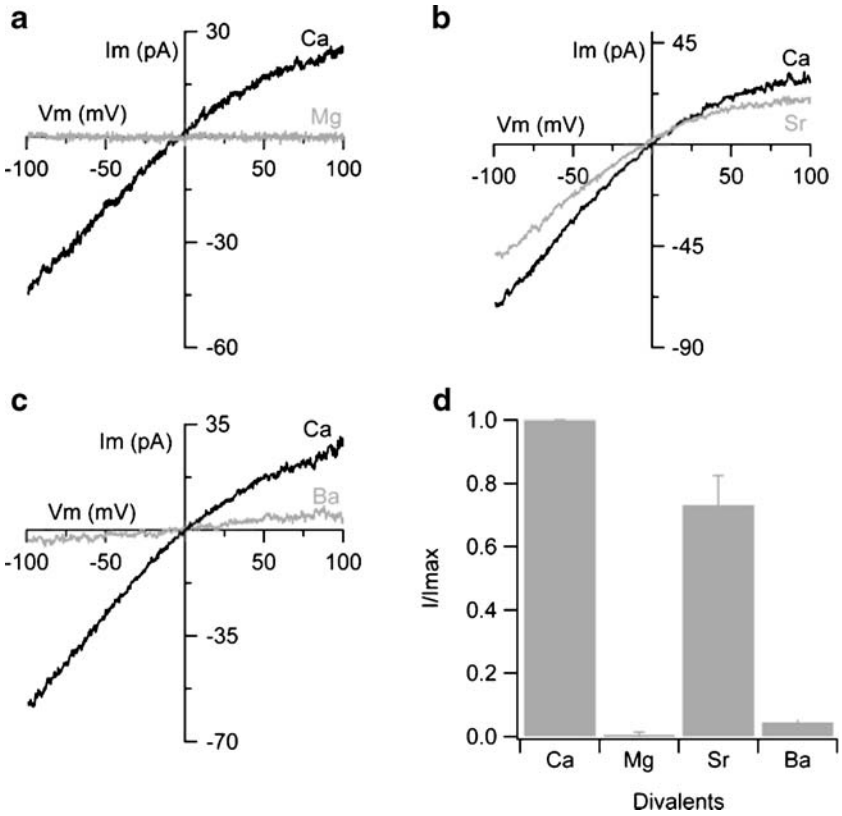

Fig. 11 Activation of mTMEM16B-mediated currents by divalent cations. An inside-out membrane patch was excised from HEK 293T cells transfected with mTMEM16B and the cytoplasmic side was exposed to 1 mM Ca^{2+} (*black traces*) or other divalent cations (*gray traces*): **a** Mg^{2+}, **b** Sr^{2+}, and **c** Ba^{2+}. *Black traces* are the average currents activated by 1 mM Ca^{2+} applied before and after each test divalent cations. Leakage currents measured in 0 divalent cations were subtracted. Current traces were from the same patch. **d** Currents activated by different divalent cations at −50 mV were normalized to the average current activated by 1 mM Ca^{2+} measured before and after each test divalent cation (n=4–5; p<0.01, t test)

did not have any effect. Also the reducing agent DTT failed to prevent the rundown, suggesting that this phenomenon is not due to oxidation of some protein residues. Since previous studies indicated that calmodulin may regulate the activation of some Ca^{2+}-activated Cl^- channels [17, 32], we also added calmodulin, but did not observe any change in the rundown. Finally, we tested cAMP, a second messenger, and PIP_3, an important cofactor of many ion channels [7, 31, 44], but none

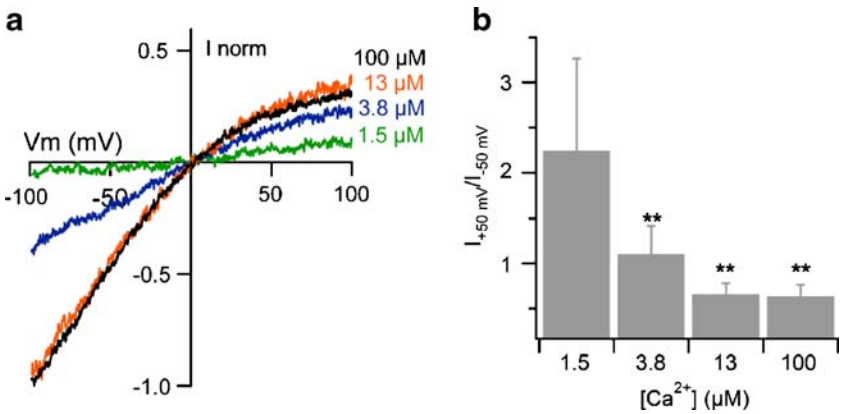

Fig. 12 Rectification of mTMEM16B-mediated currents at various Ca^{2+} concentrations. **a** Currents were activated in the same patch with voltage ramps at different Ca^{2+} concentrations and normalized to the current activated by 100 μM Ca^{2+} at −100 mV. Leakage currents measured in 0 Ca^{2+} were subtracted. Current traces were from the same patch. **b** Ratios between currents measured at +50 and at −50 mV at various Ca^{2+} concentrations (n=6; **p<0.01, ANOVA, F=11.4, p=1.4×10^{-4} followed by Tukey test)

of them significantly modified the rundown of the mTMEM16B-induced current.

In contrast to experiments with excised patches, rundown was not observed in whole-cell recordings (Fig. 1h), indicating that a still unknown modulatory mechanism can maintain a high level of activity of mTMEM16B in intact HEK 293T cells. Since channel activity decreased in cell-free conditions, it is likely that the lost factor is soluble in the cytosol. It is worth to note here that also some native Ca^{2+}-activated Cl^- channels present a rundown in activity after patch excision [16, 39, 47, 48], indicating that this phenomenon is not specifically due to channel expression in HEK 293T cells. Future studies will have to clarify the molecular determinants of this behavior.

Comparison between currents induced by mTMEM16B and TMEM16A

At present, TMEM16A is the only member of the TMEM16 family that has been electrophysiologically characterized in some detail in inside-out membrane patches after expression in HEK 293T cells [54]. We therefore compare here the functional properties of the only two members of the family that have been studied up to now: TMEM16A and mTMEM16B. Dose–response experiments for mTMEM16B showed that currents were half-maximal at a Ca^{2+} concentration of 4.0 μM at +60 mV, while at −60 mV a higher Ca^{2+} concentration of 5.1 μM was necessary to reach 50% of the maximal current, indicating that activation by Ca^{2+} is voltage-dependent (Fig. 10). A voltage-dependent Ca^{2+} sensitivity in the micromolar range was also measured in inside-out membrane patches from HEK 293T cells expressing TMEM16A [54]: at +60 mV $K_{1/2}$ for Ca^{2+} was 0.4 μM, while at −60 mV, it increased to 2.6 μM. Therefore, although both channels are activated in the micromolar range, their $K_{1/2}$ for Ca^{2+} differs of about one order of magnitude at positive potentials, indicating that their voltage dependence is different. Moreover, it has been reported that TMEM16A was inhibited by Ca^{2+} concentrations higher than 10 μM [54], whereas we did not observe any inhibition of mTMEM16B up to 100 μM Ca^{2+}. However, Fig. 3a of Yang et al. [54] shows that exposures to Ca^{2+} of inside-out membrane patches from cells expressing TMEM16A were obtained with a very slow perfusion and, moreover, the membrane patch was held for more than a minute in every Ca^{2+} concentration. It is therefore possible that the inhibition at high Ca^{2+} concentration observed with TMEM16A was due to a rundown effect similar to what we observed in mTMEM16B (Fig. 5), although this phenomenon has not been investigated in TMEM16A [54].

When Ca^{2+} concentration at the cytoplasmic side of a patch excised from a HEK 293T cell expressing TMEM16A was reduced to 0.5 μM, single-channel events were clearly distinguishable, and the single-channel conductance was 8.6 pS (Fig. 3c, d of [54]). In cells expressing mTMEM16B, we could not detect any single-channel events by lowering Ca^{2+} concentration, and therefore, we estimated the single-channel conductance from the ratio between current variance and mean current at 1.5 μM Ca^{2+}. The estimated single-channel conductance for mTMEM16B was 1.2 pS, much smaller than the value of 8.6 pS measured for TMEM16A [54].

Current–voltage relations from whole-cell recordings for TMEM16A showed a change in rectification from linear to outward when currents were measured at different times of the response induced by release of intracellular Ca^{2+} (see Fig. 2a of [54]). The variation from linear to outward rectification was consistent with previous reports on native Ca^{2+}-activated Cl^- channels at high or low Ca^{2+} concentrations, respectively [1, 9]. In whole-cell recordings from HEK 293T cells expressing mTMEM16B, we also measured a change in rectification from outward at low Ca^{2+} concentration to linear at high Ca^{2+} concentration (Fig. 1d, f). In inside-out membrane patches mTMEM16B-induced currents displayed a Ca^{2+}-dependent rectification that was outward at low Ca^{2+} concentration, linear at intermediate Ca^{2+} levels, and inward at high Ca^{2+} concentrations (Fig. 12). In inside-out patches from cells expressing TMEM16A, a change of rectification was not observed up to 3 μM Ca^{2+} (see Fig. 3a of [54]). It will be interesting to determine whether the absence of rectification change for TMEM16A in inside-out patches was due to a different range of Ca^{2+} concentrations or to a functional difference between TMEM16A and mTMEM16B.

A comparison between the pharmacological profile of whole-cell currents induced by TMEM16A and mTMEM16B shows that both currents were blocked by the extracellular application of NFA, NPPB, and DIDS [8, 51, 54].

It is of interest to note that the analysis of the sequence of both of these proteins does not reveal any typical Ca^{2+}-binding site, and therefore, the identification of the region of Ca^{2+}-binding site will be of great interest.

Comparison with native Ca^{2+}-activated Cl^- channels

Several native Ca^{2+}-activated Cl^- currents have a Ca^{2+} sensitivity in the micromolar range (for reviews, see [10, 13]), similarly to TMEM16A [54] and mTMEM16B (Fig. 10). Although such a high Ca^{2+} concentration at the bulk level is not physiological, activation is likely to occur through Ca^{2+} signaling processes that produce high local Ca^{2+} levels in subcellular domains (for review, see [30]).

A comparison of our electrophysiological data on mTMEM16B-induced currents with those of native Ca^{2+}-activated Cl^- currents in sensory neurons of the olfactory epithelium indicates that the properties of the two channels

are remarkably similar when measured in inside-out membrane patches. Studies in the mouse [45, 48] have shown that the dose–response relation of Ca^{2+}-activated Cl^- currents is well fit by the Hill equation with half-maximal activation in the micromolar range. At −50 mV, the $K_{1/2}$ for Ca^{2+} was 4.7 μM (see Fig. 4f in [45]), whereas at +50 mV, it was 2.6 μM (Pifferi, unpublished data), similar to the values for mTMEM16B of 4.9 μM at −50 mV and 3.3 μM at +50 mV measured in the present study (Fig. 10). The estimated single-channel conductance for mTMEM16B, 1.2 pS, is also similar to the value of 1.6 pS in mouse olfactory sensory neurons [45]. At high Ca^{2+} levels (100 μM), the olfactory channel showed an inward rectification, with a ratio of the current at +50 mV and at −50 mV of 0.61 (see Fig. 5d in [45]), similar to the value of 0.58 for mTMEM16B at 100 μM Ca^{2+} (Fig. 12b). In addition, when measured in inside-out patches, the olfactory Ca^{2+}-activated Cl^- current shows a reversible Ca^{2+}-dependent inactivation and an irreversible rundown, indicating that, as for mTMEM16B in HEK 293T cells, some unknown modulatory component of the channel may be lost after the excision of the membrane [47, 48].

The pharmacological profile of the olfactory Ca^{2+}-activated Cl^- channels has been investigated in detail only by the application of Cl^- channel inhibitors at the cytoplasmic face of isolated olfactory cilia from the frog [24, 26]. The percentage of inhibition of the native olfactory channel was 90% for 300 μM NFA, 78% for 300 μM FA, 32% for 300 μM NPPB, 30% for 5 mM SITS, and 5% for 100 μM DIDS (see Table 2 of [10]), to be compared with the similar percentage of inhibition obtained in this study for mTMEM16B: 99% for 300 μM NFA, 62% for 300 μM FA, 19% for 100 μM NPPB, 20% for 5 mM SITS, and 0% for 1 mM DIDS.

Moreover, NFA (300–500 μM; [6, 33, 48]) and SITS (2–5 mM; [27, 28, 33]) are often used as extracellular blockers of Ca^{2+}-activated Cl^- channels in intact olfactory sensory neurons, whereas the extracellular blocking effect of other compounds are still unknown. mTMEM16B-mediated currents in the whole-cell configuration were blocked by the extracellular application of NFA and SITS, similarly to the native olfactory channel.

Thus, the comparison of the electrophysiological properties of mTMEM16B-induced currents with those of native olfactory Ca^{2+}-activated Cl^- channels indicates that the two channels are remarkably similar.

Furthermore, a previous study showed, by in situ hybridization, that mTMEM16B is expressed in the mature sensory neurons of the olfactory epithelium [55], and a more recent study demonstrated that TMEM16B is a prominent protein in the olfactory ciliary proteome [35]. At present, the molecular identity of the olfactory channel is still elusive and, before the reports indicating that the TMEM16 family could form Ca^{2+}-activated Cl^- channels [8, 51, 54], the protein bestrophin-2 was the best candidate for being a molecular component of the olfactory conductance [45]. Indeed, it has been shown that bestrophin-2 is expressed in the cilia, at the site of olfactory transduction, and that its functional properties have many similarities with those of the native olfactory channel, although some differences have also been pointed out [45]. One significant variation between the two currents is a Ca^{2+}-sensitivity difference of one order of magnitude: at −50 mV currents were half-maximal at a Ca^{2+} concentration of 0.4 μM for bestrophin-2, whereas native currents required a higher Ca^{2+} concentration of 4.7 μM [45]. As previously discussed in detail, we showed in this study that the functional properties of mTMEM16B-induced currents are very similar to those of the native Ca^{2+}-activated Cl^- olfactory channel, including a similar Ca^{2+} sensitivity. Thus, at present, the identification of mTMEM16B in the olfactory ciliary proteome [35], together with the electrophysiological properties, suggests that mTMEM16B is the best candidate for being the main molecular component of the native olfactory Ca^{2+}-activated Cl^- channel.

Further studies combining a multidisciplinary approach from genetic and molecular biology and electrophysiology will have to reveal the physiological role of mTMEM16B and of the other members of this newly discovered family of proteins.

Acknowledgments We thank Lara Masten, Giulia Betto, and Fulvio Celsi for their help in some experiments. This study was supported by grants from the Italian Ministry of Research (MIUR) and from the Italian Institute of Technology.

References

1. Arreola J, Melvin J, Begenisich T (1996) Activation of calcium-dependent chloride channels in rat paroid acinar cells. J Gen Physiol 108:35–47
2. Arreola J, Melvin JE, Begenisich T (1998) Differences in regulation of Ca^{2+}-activated Cl^- channels in colonic and parotid secretory cells. Am J Physiol 274:C161–C166
3. Bader CR, Bertrand D, Schwartz EA (1982) Voltage-activated and calcium-activated currents studied in solitary rod inner segments from the salamander retina. J Physiol 331:253–284
4. Barish ME (1983) A transient calcium-dependent chloride current in the immature Xenopus oocyte. J Physiol 342:309–325
5. Bers DM (2008) Calcium cycling and signaling in cardiac myocytes. Annu Rev Physiol 70:23–49
6. Boccaccio A, Menini A (2007) Temporal development of cyclic nucleotide-gated and Ca2+-activated Cl^- currents in isolated mouse olfactory sensory neurons. J Neurophysiol 98:153–160
7. Brady JD, Rich ED, Martens JR, Karpen JW, Varnum MD, Brown RL (2006) Interplay between PIP3 and calmodulin regulation of olfactory cyclic nucleotide-gated channels. Proc Natl Acad Sci U S A 103:15635–15640
8. Caputo A, Caci E, Ferrera L, Pedemonte N, Barsanti C, Sondo E, Pfeffer U, Ravazzolo R, Zegarra-Moran O, Galietta LJ (2008) TMEM16A, a membrane protein associated with calcium-dependent chloride channel activity. Science 322:590–594

9. Evans MG, Marty A (1986) Calcium dependent chloride currents in isolated cells from rat lacrimal glands. J Physiol 378:437–460
10. Frings S, Reuter D, Kleene SJ (2000) Neuronal Ca2+-activated Cl^- channels—homing in on an elusive channel species. Prog Neurobiol 60:247–289
11. Galindo BE, Vacquier VD (2005) Phylogeny of the TMEM16 protein family: some members are overexpressed in cancer. Int J Mol Med 16:919–924
12. Hamann M, Gibson A, Davies N, Jowett A, Walhin JP, Partington L, Affleck K, Trezise D, Main M (2009) Human ClCa1 modulates anionic conduction of calcium dependent chloride currents. J Physiol 587:2255–2274. doi:10.1113/jphysiol.2009.170159
13. Hartzell C, Putzier I, Arreola J (2005) Calcium-activated chloride channels. Annu Rev Physiol 67:719–758
14. Hartzell HC, Yu K, Xiao Q, Chien LT, Qu Z (2008) Anoctamin/TMEM16 family members are Ca^{2+}-activated Cl^- channels. J Physiol 587:2127–2139. doi:10.1113/jphysiol.2008.163709
15. Hille B (2001) Ion channels of excitable membranes. Sinauer Associates, Sunderland, MA
16. Hirakawa Y, Gericke M, Cohen RA, Bolotina VM (1999) Ca^{2+}-dependent Cl^- channels in mouse and rabbit aortic smooth muscle cells: regulation by intracellular Ca^{2+} and NO. Am J Physiol Heart Circ Physiol 277:H1732–H1744
17. Kaneko H, Mohrlen F, Frings S (2006) Calmodulin contributes to gating control in olfactory calcium-activated chloride channels. J Gen Physiol 127:737–748
18. Katoh M, Katoh M (2003) FLJ10261 gene, located within the CCND1-EMS1 locus on human chromosome 11q13, encodes the eight-transmembrane protein homologous to C12orf3, C11orf25 and FLJ34272 gene products. Int J Oncol 22:1375–1381
19. Katoh M, Katoh M (2004) Characterization of human TMEM16G gene in silico. Int J Mol Med 14:759–764
20. Katoh M, Katoh M (2004) GDD1 is identical to TMEM16E, a member of the TMEM16 family. Am J Hum Genet 75:927–928
21. Katoh M, Katoh M (2004) Identification and characterization of human TP53I5 and mouse Tp53i5 genes in silico. Int J Oncol 25:225–230
22. Katoh M, Katoh M (2004) Identification and characterization of TMEM16E and TMEM16F genes in silico. Int J Oncol 24:1345–1349
23. Katoh M, Katoh M (2005) Identification and characterization of TMEM16H gene in silico. Int J Mol Med 15:353–358
24. Kleene SJ (1993) Origin of the chloride current in olfactory transduction. Neuron 11:123–132
25. Kleene SJ (2008) The electrochemical basis of odor transduction in vertebrate olfactory cilia. Chem Senses 33:839–859
26. Kleene SJ, Gesteland RC (1991) Calcium-activated chloride conductance in frog olfactory cilia. J Neurosci 11:3624–3629
27. Kurahashi T, Menini A (1997) Mechanism of odorant adaptation in the olfactory receptor cell. Nature 385:725–729
28. Kurahashi T, Yau KW (1993) Co-existence of cationic and chloride components in odorant-induced current of vertebrate olfactory receptor cells. Nature 363:71–74
29. Kuruma A, Hartzell HC (2000) Bimodal control of a Ca(2+)-activated Cl(−) channel by different Ca(2+) signals. J Gen Physiol 115:59–80
30. Laude AJ, Simpson AW (2009) Compartmentalized signalling: Ca^{2+} compartments, microdomains and the many facets of Ca^{2+} signalling. FEBS J 276:1800–1816
31. Le Blanc C, Mironneau C, Barbot C, Henaff M, Bondeva T, Wetzker R, Macrez N (2004) Regulation of vascular L-type Ca2+ channels by phosphatidylinositol 3, 4, 5-trisphosphate. Circ Res 95:300–307
32. Leblanc N, Ledoux J, Saleh S, Sanguinetti A, Angermann J, O'Driscoll K, Britton F, Perrino BA, Greenwood IA (2005) Regulation of calcium-activated chloride channels in smooth muscle cells: a complex picture is emerging. Can J Physiol Pharmacol 83:541–556
33. Lowe G, Gold GH (1993) Nonlinear amplification by calcium-dependent chloride channels in olfactory receptor cells. Nature 366:283–286
34. Marty A, Tan YP, Trautmann A (1984) Three types of calcium-dependent channel in rat lacrimal glands. J Physiol 357:293–325
35. Mayer U, Küller A, Daiber PC, Neudorf I, Warnken U, Schnölzer M, Frings S, Möhrlen F (2009) The proteome of rat olfactory sensory cilia. Proteomics 9:322–334
36. Melvin JE, Yule D, Shuttleworth T, Begenisich T (2005) Regulation of fluid and electrolyte secretion in salivary gland acinar cells. Annu Rev Physiol 67:445–469
37. Miledi R (1982) A calcium-dependent transient outward current in *Xenopus laevis* oocytes. Proc R Soc Lond B Biol Sci 215:491–497
38. Miledi R, Parker I (1984) Chloride current induced by injection of calcium into Xenopus oocytes. J Physiol 357:173–183
39. Morris AP, Frizzell RA (1993) Ca^{2+}-dependent Cl^- channels in undifferentiated human colonic cells (HT-29). II. Regulation and rundown. Am J Physiol Cell Physiol 264:C977–C985
40. Otowa T, Yoshida E, Sugaya N, Yasuda S, Nishimura Y, Inoue K, Tochigi M, Umekage T, Miyagawa T, Nishida N, Tokunaga K, Tanii H, Sasaki T, Kaiya H, Okazaki Y (2009) Genome-wide association study of panic disorder in the Japanese population. J Hum Genet 54:122–126
41. Patton C, Thompson S, Epel D (2004) Some precautions in using chelators to buffer metals in biological solutions. Cell Calcium 35:427–431
42. Petersen OH (2005) Ca^{2+} signalling and Ca^{2+}-activated ion channels in exocrine acinar cells. Cell Calcium 38:171–200
43. Petersen OH, Tepikin AV (2008) Polarized calcium signaling in exocrine gland cells. Annu Rev Physiol 70:273–299
44. Pian P, Bucchi A, Robinson RB, Siegelbaum SA (2006) Regulation of gating and rundown of HCN hyperpolarization-activated channels by exogenous and endogenous PIP2. J Gen Physiol 128:593–604
45. Pifferi S, Pascarella G, Boccaccio A, Mazzatenta A, Gustincich S, Menini A, Zucchelli S (2006) Bestrophin-2 is a candidate calcium-activated chloride channel involved in olfactory transduction. Proc Natl Acad Sci U S A 103:12929–12934
46. Qu Z, Hartzell HC (2000) Anion permeation in Ca(2+)-activated Cl(−) channels. J Gen Physiol 116:825–844
47. Reisert J, Bauer PJ, Yau KW, Frings S (2003) The Ca-activated Cl channel and its control in rat olfactory receptor neurons. J Gen Physiol 122:349–363
48. Reisert J, Lai J, Yau KW, Bradley J (2005) Mechanism of the excitatory Cl^- response in mouse olfactory receptor neurons. Neuron 45:553–561
49. Rock JR, Harfe BD (2008) Expression of TMEM16 paralogs during murine embryogenesis. Dev Dyn 237:2566–2574
50. Schneppenheim R, Castaman G, Federici AB, Kreuz W, Marschalek R, Oldenburg J, Oyen F, Budde U (2007) A common 253-kb deletion involving VWF and TMEM16B in German and Italian patients with severe von Willebrand disease type 3. J Thromb Haemost 5:722–728
51. Schroeder BC, Cheng T, Jan YN, Jan LY (2008) Expression cloning of TMEM16A as a calcium-activated chloride channel subunit. Cell 134:1019–1029
52. Tsutsumi S, Kamata N, Vokes TJ, Maruoka Y, Nakakuki K, Enomoto S, Omura K, Amagasa T, Nagayama M, Saito-Ohara F, Inazawa J, Moritani M, Yamaoka T, Inoue H, Itakura M (2004) The novel gene encoding a putative transmembrane protein is mutated in gnathodiaphyseal dysplasia (GDD). Am J Hum Genet 74:1255–1261
53. Wray S, Burdyga T, Noble K (2005) Calcium signalling in smooth muscle. Cell Calcium 38:397–407
54. Yang YD, Cho H, Koo JY, Tak MH, Cho Y, Shim WS, Park SP, Lee J, Lee B, Kim BM, Raouf R, Shin YK, Oh U (2008) TMEM16A confers receptor-activated calcium-dependent chloride conductance. Nature 455:1210–1215
55. Yu TT, McIntyre JC, Bose SC, Hardin D, Owen MC, McClintock TS (2005) Differentially expressed transcripts from phenotypically identified olfactory sensory neurons. J Comp Neurol 483:251–262